NJC

ROYAL SOCIETY OF CHEMISTRY

PAPER

View Article Online
View Journal | View Issue

Cite this: *New J. Chem.*, 2024, **48**, 8578

From byproducts to NLO-active dyes: catalyst-free transfer hydrogenation in the modular synthesis of merocyanines†

Jie Zou,‡[abc] Yi Pan,‡[b] Di Zhang,[abc] Jie Zhang,[ab] Weilong Chen,[abc] Hongyan Sun,[ab] Kai-Chung Lau *[b] and Jingdong Luo *[abc]

Received 20th February 2024,
Accepted 8th April 2024

DOI: 10.1039/d4nj00820k

rsc.li/njc

We report an unexpected direct transfer hydrogenation (TH) from 8-alkoxyjulolidine as a strong electron donor to tricyanofuran-based hemicyanines and tandem condensation for the synthesis of push–pull chromophores. Density functional theory calculations identify the α-hydride transfer of julolidine derivatives, instead of nucleophilic addition, as the key initial step of reaction cascades, followed by efficient β-deprotonation to generate a nucleophilic enamine of isojuloline that condenses *in situ* with a second equivalent of hemicyanines as electrophiles. The scheme represents an exceptional example of TH reactions from 8-alkoxyjulolidine to highly polarizable hemicyanines, notably under simple reaction conditions without using potent catalysts of metal complexes or Lewis acids. The resulting products of isojuloline-based merocyanines exhibit strong near-infrared (NIR) absorption and large first hyperpolarizabilities. The study suggests that direct TH can be exploited to construct new NIR merocyanines by following rational, regioselective condensation pathways for photonic applications.

Introduction

Transfer hydrogenation (TH) is a chemical reaction in which a hydride or proton is transferred from an organic hydrogen donor to a polar unsaturated compound, such as ketones, imines, and alkenes. Recently TH has emerged as a safer and more convenient method alternative to the traditional hydrogenation methods by eliminating the use of flammable hydrogen gas and high-pressure hydrogenation reactors.[1–3] However, until now TH reactions of C=C double bonds from tertiary amines remain unreported, due to limited polarizability of alkenes and challenge in activating or eliminating both the α- and β-C(sp^3) hydrogens of the nitrogen atom.[3–6]

Only very few methods have been reported to enable the TH reactions from tertiary amines, such as by reacting diethyl azodicarboxylate (DEAD) with tertiary amines through nucleophilic addition to form zwitterionic intermediates (Fig. 1A),[4] or by selecting elegant noble/transition metal complexes (Fig. 1B).[5] Furthermore, beyond a better synthetic capability in constructing molecular complexity is the lack of examples using TH-enabled reactions in the synthesis of amine-containing functional molecules and molecular materials. Most tertiary amine

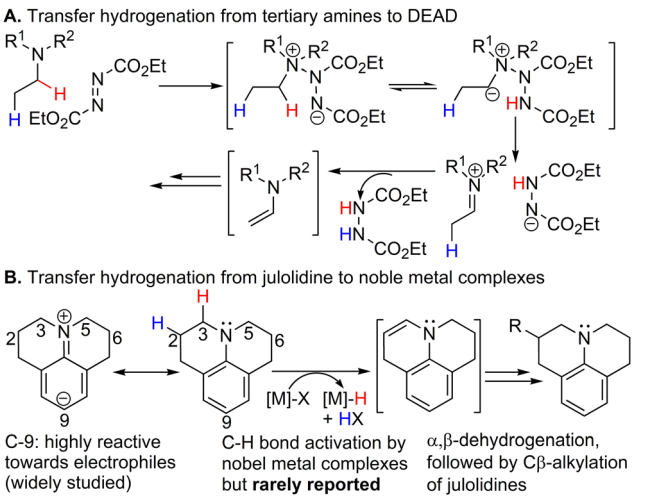

Fig. 1 (A) Dehydrogenation of tertiary amines involving nucleophile addition with DEAD and subsequent hydrogen transfers; (B) TH from julolidine to noble metal catalysts, plus the normal C-9 nucleophilicity of julolidines.

[a] *Shenzhen Research Institute, City University of Hong Kong, Shenzhen 518057, China*
[b] *Department of Chemistry, City University of Hong Kong, Kowloon, Hong Kong SAR, China. E-mail: kaichung@cityu.edu.hk, jingdluo@cityu.edu.hk*
[c] *Hong Kong Institute for Clean Energy, City University of Hong Kong, Kowloon, Hong Kong SAR, China*

† Electronic supplementary information (ESI) available: Computational details, synthetic schemes, experimental section, spectra, and X-ray crystallography. CCDC 2289992–2289995. For ESI and crystallographic data in CIF or other electronic format see DOI: https://doi.org/10.1039/d4nj00820k

‡ These authors contributed equally.

products were obtained through addition reactions to the sp^2 carbon of iminium or enamine intermediates, keeping the sp^3 hybridization for the carbon centers unchanged after the transformation (Fig. 1B).[4–7] Therefore, it is highly desirable to functionalize the tertiary anilines as the electron donor of π-conjugated molecules through efficient TH reactions of polarizable olefins, which would mark a significant step toward the exploration of new molecular structures for potential applications in nonlinear optics,[8–10] fluorescent bioimaging,[11,12] and phototheranostics.[13,14]

In the meantime there is growing interest in concise synthesis of push–pull polymethines containing the tricyanofuran (TCF) acceptors for photonic applications (Fig. 2A–C).[8–10,15] Many researchers are particularly interested in the study of modular reaction sequences, consisting of consecutive multiple-step, one-pot reactions, for efficient synthesis of key intermediates and push–pull chromophores. In our quest of simple and highly efficient synthetic protocols for new TCF-based push–pull structures, the present work was initiated in studying the feasibility of direct condensation between the julolidine donors and TCF-based hemicyanine precursors, which are considered as among the most widely used conjugated units with structural diversity and synthetic scalability.[8–10,15–18] Following the condensation with methylene bases, we expected that the C-9 position of the substituted phenyl ring would be the predominant nucleophilic site for julolidines to react with π-conjugated TCF hemicyanines and form type-I products under normal conditions (Path I, Fig. 2D). Interestingly, we obtained an unexpected major product (type-II product) of a fully π-conjugated push–pull structure containing an isojuloline donor, π-conjugated bridge, and TCF acceptor (Path II, Fig. 2D), in which the isojuloline group is the dehydrogenated product from the julolidine substrate.

The above critical literature review and preliminary findings motivated us to conduct this study for new push–pull molecules to understand the mechanisms of tandem reactions and material properties. We have investigated the TH from 8-alkoxyjulolidine as a strong electron donor to π-conjugated TCF-type hemicyanines and tandem condensation for the synthesis of push–pull chromophores, as well as the effect of acceptor substituents on regioselectivity of two distinct pathways (Fig. 2D). Density-functional theory (DFT) calculations and spectroscopic analyses demonstrate that the TH process involves direct transfer of both α and β hydrogens of 8-alkoxyjulolidine to the C=C double bond of highly polarizable TCF-type hemicyanines, notably under simple reaction conditions without using potent catalysts of noble metal complexes or forming very reactive intermediates through nucleophilic addition (Fig. 1). The formed isojuloline intermediate can be condensed with TCF acceptor precursors *in situ* to access fully π-conjugated push–pull structures. The discovery of this new method has the potential to overcome the issues of non-conjugated functionalization of amine donors through TH and narrow substrate scope under harsh reaction additions and synthesize diverse push–pull chromophores that could not otherwise be obtained.

Results and discussion

Preliminary synthesis

We selected the 1,1,7,7-tetramethyl-substituted 8-butoxyjulolidine donor (**JD1**) and the hemicyanine consisting of a π-conjugated trienyl precursor with a terminal TCF acceptor group (hereafter **TCF-A1**), two widely used building blocks for push–pull chromophores,[8–10,15–18] to start the study (Fig. 3). The common condensation protocols for the synthesis of merocyanines and cyanines have been followed to optimize the reaction conditions and identify the structures of major chromophore products (Table 1). All the new chromophores were characterized by ^{1}H NMR, ^{13}C NMR, high-resolution mass spectrometry (HRMS), cyclic voltammograms, UV-vis-NIR spectroscopy, and thermogravimetric analysis (TGA).

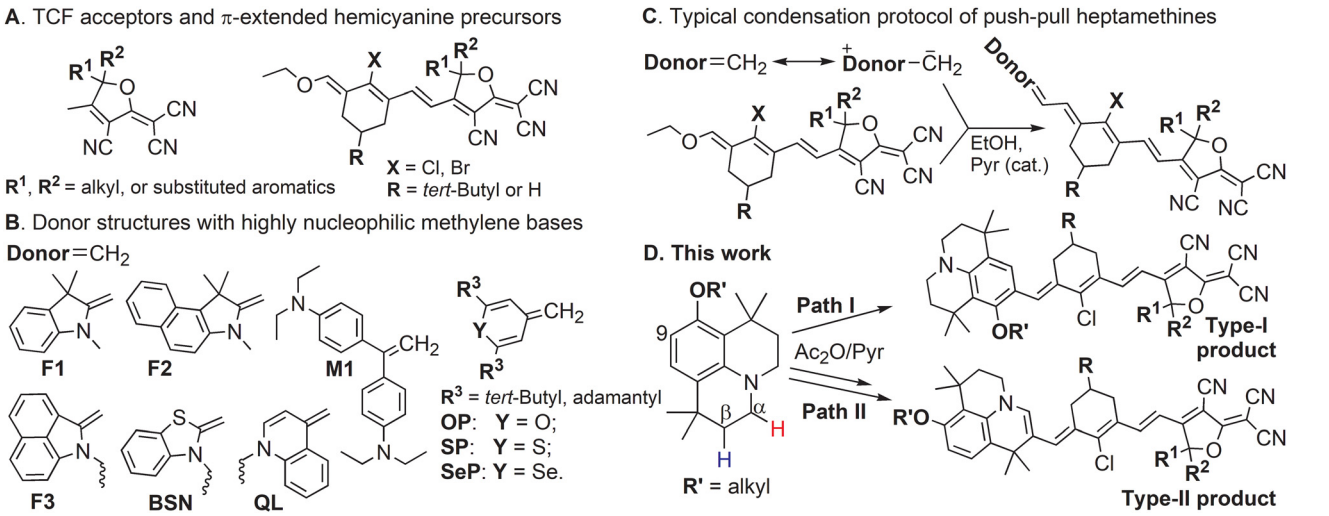

Fig. 2 Molecular structures and modular synthesis of push–pull heptamethines containing TCF-acceptor precursors and heterocyclic donors, and new regioselective condensation pathways accomplished in this study for photonic applications.

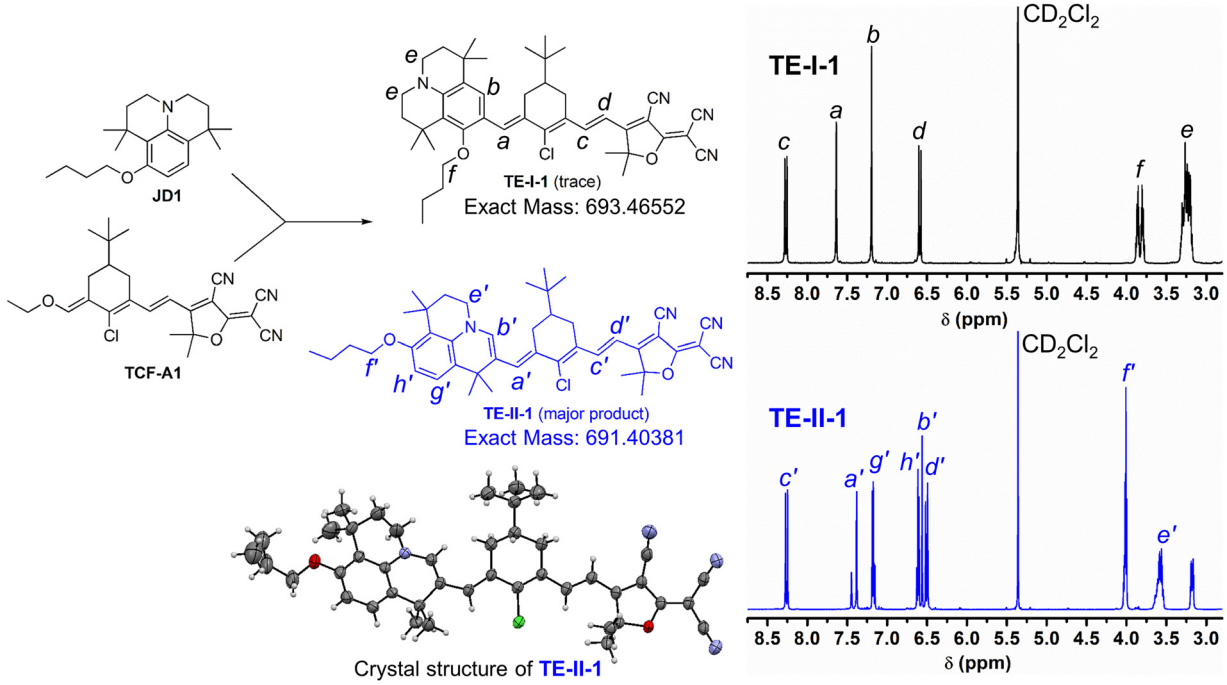

Fig. 3 Molecular structures and concise synthesis of push–pull heptamethines containing TCF-acceptor precursors and heterocyclic donors, and new regioselective condensation pathways accomplished in this study for photonic applications.

Table 1 Optimization of reaction conditions between **JD1** and **TCF-A1**

Entry	Solvent	JD1/TCF-A1 ratio	Temp. (°C)	Time (h)	Yield (%) TE-I-1	Yield (%) TE-II-1
1	Ethanol	1.1	70	72	Trace	15
2	Ac_2O	1.1	80	14	3	27
3	Ac_2O	0.6	80	14	2	26
4	Ac_2O	2.1	80	18	3	29
5	Ac_2O	3.1	80	18	Trace	16

In refluxing ethanol with a catalytic amount of pyridine (Pyr), we obtained only a low 15% yield of type-II push–pull tetraene "abnormal byproduct" **TE-II-1** and no "normal" product or only a trace amount of type-I phenyltriene **TE-I-1** product was detected (Table 1, entry 1). In acetic anhydride, the yields of isolated product **TE-II-1** have been improved to 26–29% by changing the reaction time and equivalence ratio of reactants, while **TE-I-1** remained the minor product (Table 1, entries 2–4). Compared to **TE-I-1**, **TE-II-1** showed two more downfield proton NMR signals of π-bonds at the expense of two upfield proton signals of the methylene group located around 3.5 ppm, plus a small amount of a geometrical isomer. The mass data and crystal structure further verified the structure of **TE-II-1**. A low yield of **TE-I-1** indicates **JD1** as a π-nucleophile is less reactive than methylene bases, such as indoline, benzoindoline, benzothiazoline, and Michler's base derivatives, in condensation with π-electrophile **TCF-A1**. This can be explained by the aromaticity and steric hindrance of **JD1** that reduces its nucleophilicity, and the unexpected dehydrogenation reactivity.

Computational assessment and experimental verification of reaction mechanisms

The "abnormal byproduct" **TE-II-1** can only be obtained by the condensation between **TCF-A1** and an *in situ* generated new enamine donor of isojuloline from the dehydrogenation of **JD1**. We explored the reaction path using a combined experimental study and density functional theory (DFT).[19–22] Since no Lewis acids or noble metal complexes were used in the synthesis of **TE-II-1**, we study the reaction mechanism and explore the potential energy surface (PES) for the formation of **TE-II-1** ("abnormal" product) and **TE-I-1** ("normal" product) at the DFT level. The transition states (**TS**) were located, and their barrier heights were calculated and compared to explain the yields of **TE-I-1** and **TE-II-1** in the synthesis.

For the formation of **TE-II-1** ("abnormal" product), there are two possible reaction pathways: (i) the nucleophilic addition (NA) of nitrogen lone pair of **JD1** to **TCF-A1** and (ii) the intermolecular hydride transfer (HT) from **JD1** to **TCF-A1**. Herein the hemicyanine **TCF-A1** could act as either a hydride acceptor or an electrophile in the reactions. Also, as reported by Li *et al.*,[4,23] the strong electrophile of DEAD can be used to form the zwitterionic adducts with the tertiary amines to activate the α and β hydrogens for further HT (Fig. 1A), which led to the analysis of the NA pathway in this study. Due to the relatively long π-conjugation bridge of **TCF-A1**, we have screened multiple carbon centers in both the HT and NA pathways. As both the **JD1** and **TCF-A1** are of considerable size, to help saving the computational cost of DFT calculations, we have (i) replaced the *n*-butoxy with a methoxy group in the **JD1**, the resultant molecule (8-methoxyjulolidine) is named as **JD1′**;

Table 2 Scope and selectivity for the reaction between julolidine derivatives (**JD#**) and π-conjugated TCF hemicyanines (**TCF-A#**)[abc]

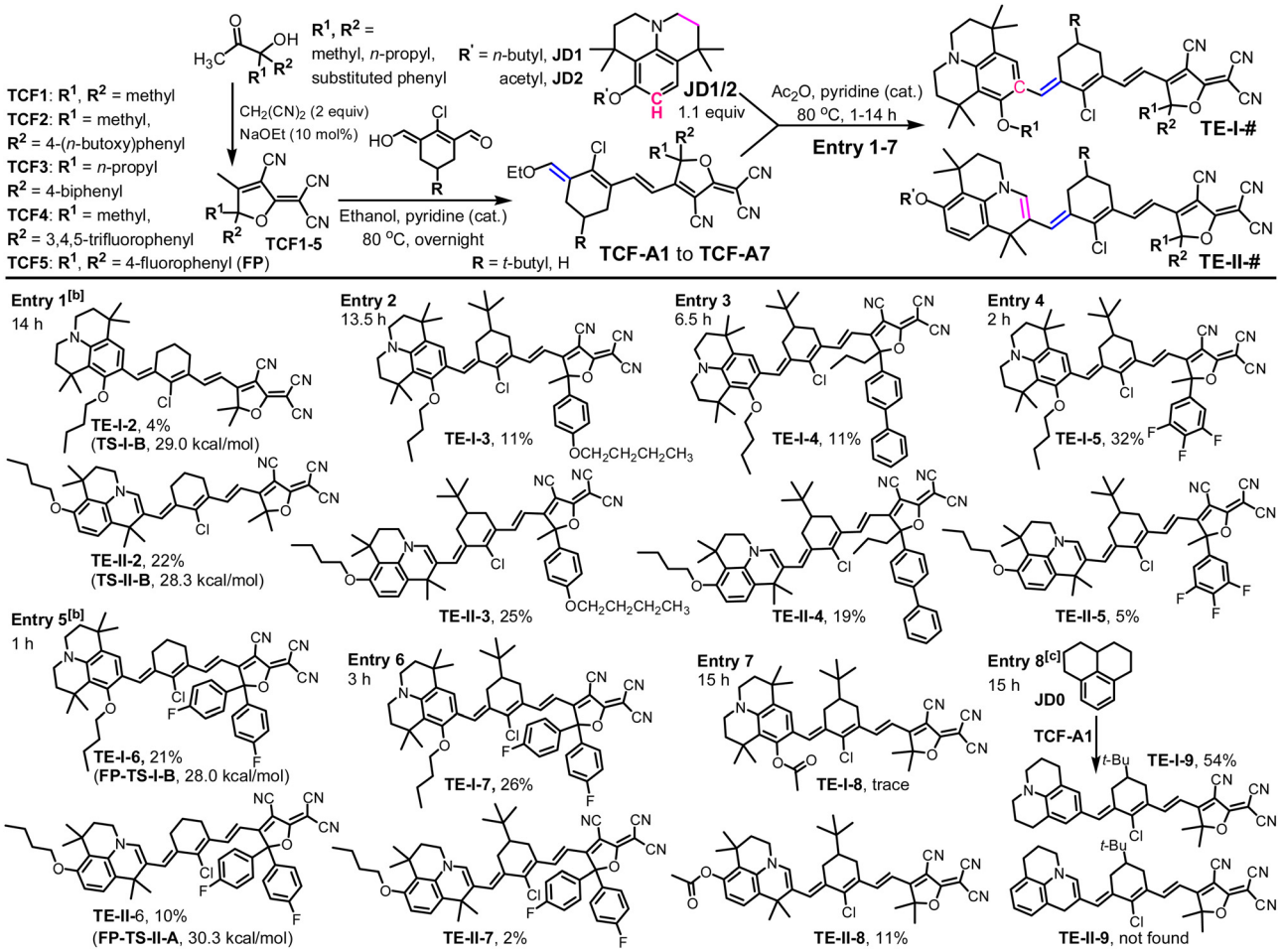

[a] The isolated product yields were reported after flash column chromatography and recrystallization. Optimized reaction time was included. [b] For entry 1 and 5, the values in parentheses are the calculated highest activation energy ($\Delta G^{\ddagger}_{298}$, kcal mol^{-1}) in acetic anhydride at the B3LYP-D3(BJ)/ma-TZVP level. The *n*-butoxy group of JD1 was replaced by the methoxy group to save computational time. See Fig. 4 and the ESI for detailed PES and structures. [c] Entry 8 uses the unsubstituted julolidine JD0 under the same reaction condition for comparison.

(ii) substituted a *t*-butyl group in the chlorocyclohexene ring of **TCF-A1** with a hydrogen, and the molecule is named **TCF-A2** (see Table 2 and Scheme S3, ESI†).

Three carbon centers (marked with an asterisk in Fig. S1, ESI†) along the conjugated double bonds of **TCF-A2** have been identified by their electrophilicity, *i.e.*, positive atomic charge, for the preliminary calculations of HT. Our preliminary single-point calculations at the B3LYP-D3(BJ)/def2-TZVP//B3LYP-D3(BJ)/def2-SVP level suggest that the HT pathway would be favored with a modest barrier of 26.5 kcal mol^{-1} by attacking the ethoxylated ethylene terminal, and 26.3 kcal mol^{-1} by attacking the central ethylene, both possibly as the initial step (Table S1, ESI†).[24–26] The HT at the dicyanovinylene terminal and NA pathway can be ruled out due to much higher barriers of 36.5 kcal mol^{-1} and 37.0 kcal mol^{-1} (Table S1, ESI†), respectively, for which considerable steric congestion can be expected.

We further explored the detailed reaction mechanism of normal C-9 condensation (Path I) and HT pathway (Path II) at the B3LYP-D3(BJ)/ma-TZVP level, for improving the accuracy of both geometrical optimizations and energy corrections, and obtained the relevant PES (Fig. 4, **TCF-A2**-based in black color) and a complete set of intermediates (**INTs**) and **TS**s for the reaction (Fig. S2, ESI†).

In Path II, the HT step firstly proceeds, starting from an hydrogen-bonded intermediate (**INT-II-A**) formed between **JD1′** and **TCF-A2**, *via* **TS-II-A** where it has two relatively short partial C···H bonds around 1.39 Å and a slightly bent Cα···H···C angle of 166.7°, likely imposed by noncovalent π–π interactions between the donor **JD1′** and acceptor **TCF-A2** (Fig. 4 red line and 3D structure of **TS-II-A**). The barrier height ($\Delta G^{\ddagger}_{298}$) of **TS-II-A** is 27.0 kcal mol^{-1}, relative to **JD1′** and **TCF-A2**. In addition, different from most tertiary amines involving HT with an sp^3-hybridized nitrogen center, the nitrogen in the **JD1′** is sp^2-hybridized to permit more efficient conjugation with the aromatic nucleus.[27] Thus the lone pair of nitrogen would impose a better stabilization effect on the α-carbocation in **TS-II-A** through resonance. The HT proceeds over **TS-II-A** to give a weakly bound complex

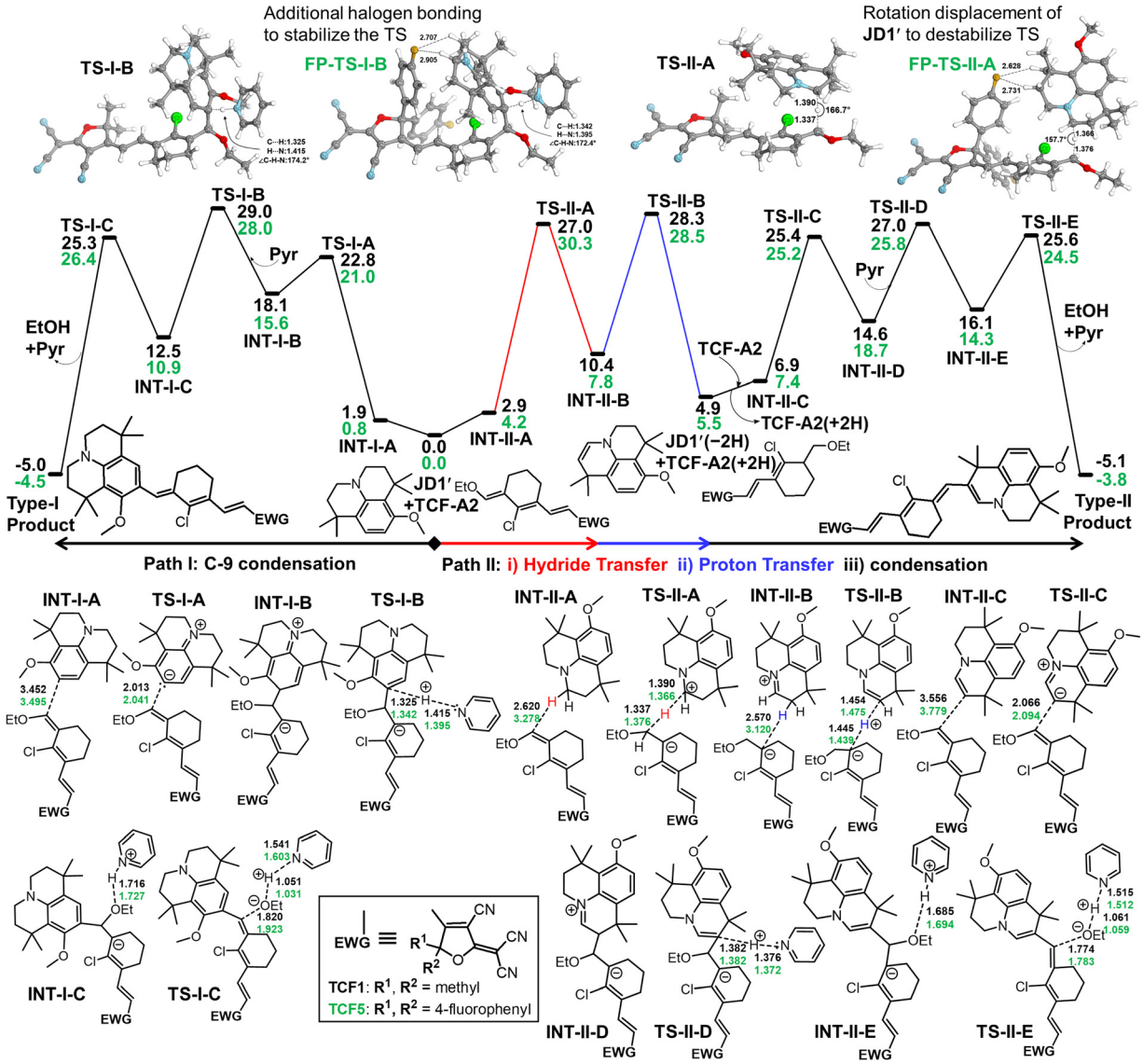

Fig. 4 PES of the reactions between simplified analogues of 8-methoxyjulolidine (**JD1′**) and TCF-based hemicyanines, **TCF-A2** (black bold font) and **TCF-A6** where R^1, R^2 is 4-fluorophenyl (**FP**, Green and bold numbers), by following the Path I or Path II to form type-I and type-II products at the B3LYP-D3(BJ)/ma-TZVP level (all values are ΔG_{298} in kcal mol^{-1}) in acetic anhydride. The 3D structures of higher-barrier transition states are shown at the top.

intermediate **INT-II-B**, which is resonance stabilized. Next, like the **TS-II-A** in HT, two short partial C···H bonds around 1.45 Å and a Cβ···H···C angle of 173.4° were found in **TS-II-B** with a $\Delta G^{\ddagger}_{298}$ value of 28.3 kcal mol^{-1}, which is slightly higher than that of **TS-II-A**. The subsequent proton transfer (PT, Fig. 4, blue line) completes the TH reaction to afford the **JD1′(−2H)**, as the dehydrogenated product **JD1′(−2H)** of **JD1′**, and **TCF-A2(+2H)** as the hydrogenated product (in terminal ethoxy-substituted ethylene) of **TCF-A2**. Then, the *in situ* generated **JD1′(−2H)** as an enamine π-nucleophile undergoes the condensation reaction with another **TCF-A2** to give the type-II product *via* several mechanistic steps starting from the intermediate (**INT-II-C**) by following the common addition/elimination pathway. The $\Delta G^{\ddagger}_{298}$ of **TS-II-C** is clearly lower than the $\Delta G^{\ddagger}_{298}$ of **TS-II-A**, suggesting that the reaction cascade would be controlled by HT or PT, depending on the substituents on the TCF acceptors, as the rate-determining step. Furthermore, the "normal" condensation (Path I) has been investigated to obtain a more thorough understanding of the reactivity of the substrates for comparison (Fig. 4, black line on the left). We obtained a somewhat higher $\Delta G^{\ddagger}_{298}$ for **TS-I-B** by 0.7 kcal mol^{-1} than that of **TS-II-B** in Path II. Given the typical uncertainty of a few kcal mol^{-1} in the current DFT level, although the difference in two $\Delta G^{\ddagger}_{298}$ values is too small to call, in fact, our predictions correlate well with the experimental results, from which the reaction equilibrium favors the product of **TE-II-2** over the **TE-I-2** by a factor of five in the isolated products (Table 2, entry 1).

In the reaction cascade *via* the central ethylene (denoted as "c") of **TCF-A2** (Fig. S3, ESI†), the respective $\Delta G^{\ddagger}_{298}$ values of HT and PT are 25.5 kcal mol^{-1} (*via* **TS-II-A(c)**) and 27.9 kcal mol^{-1}

(*via* **TS-II-B(c)**), both values are quantitatively similar to the $\Delta G^{\ddagger}_{298}$'s of the HT/PT steps *via* the terminal ethoxylated ethylene, 27.0 kcal mol^{-1} (*via* **TS-II-A**) and 28.3 kcal mol^{-1} (*via* **TS-II-B**). Upon the formation of the dehydrogenated **JD1′** and hydrogenated **TCF-A2(+2H,c)**, the generated **JD1′(−2H)** together with another **TCF-A2** would undergo the condensation reaction as usual and this reaction cascade is expected to contribute to the formation of type-II product.

The DFT calculations were validated with the experimental data for comparative purposes in a qualitative sense. The relatively high barrier suggests that the reactions would hardly proceed at room temperature. At the elevated temperature in acetic anhydride, the change of **JD1**/**TCF-A1** ratio from 0.6 to 2.1 gave essentially the same yield (∼27%) of **TE-II-1** with trace amount of **TE-I-1** (Table 1, entries 2–4). This underscores the dual role of hydrophilicity and electrophilicity of **TCF-A1** hemicyanine, especially in the rate-determining step of HT. Besides the final products, we were able to collect the byproduct of hydrogenated **TCF-A1(+2H)** using HPLC and further verify it by HRMS as explicit experimental evidence (Fig. S5, ESI†). It is worth noting that this result was obtained after many trial reactions in order to capture trace amounts of **TCF-A1(+2H)** as a highly unstable intermediate under the reaction conditions. In controlled experiments at 80 °C, without adding **TCF-A1**, **JD1** stayed unreacted in acetic anhydride with a catalytic amount of pyridine, corroborating the TH from **JD1** to **TCF-A1**, not to the acetic anhydride. Without pyridine, neither **TE-II-1** nor **TE-I-1** were obtained by simply mixing **JD1** and **TCF-A1** in acetic anhydride, supporting the key role of pyridine as a base catalyst for deprotonation in condensation. The DFT calculations predicted a little lower $\Delta G^{\ddagger}_{298}$ value for Path II than that of Path I, reflecting a preliminary selectivity of two competing pathways to afford **TE-II-1** as the major product over **TE-I-1**. As a matter of fact, our calculations in this study use a simplified molecular model (**JD1′** and **TCF-A2**) to mimic the actual reactants. It is worth noting that the isolated product yield of 27% for **TE-II-1** in this one-pot, two-step cascade reaction indicates a modest yield roughly around 50% in the critical intermolecular TH reaction *via* sequential HT and PT, which is considered a remarkable result without using potent catalysts of noble metal complexes or Lewis acids.

Influence of the donors and acceptors in the reactions

Next, we investigated the scope and selectivity of the reactions between julolidine derivatives and π-conjugated TCF hemicyanines (Table 2 and Tables S2–S6, ESI†). We included the simplest julolidine **JD0** and two commonly used 1,1,7,7-tetramethyljulolidine donors **JD1-2** with 8-*n*-butoxy and 8-acetoxy groups, respectively. A series of TCF acceptors (**TCF1-5**) were synthesized through newly developed two consecutive, multiple step, one-pot reactions, for which the acceptor strength and steric hindrance can be tuned by introducing the germinal substituents of $\mathbf{R^1}$ and $\mathbf{R^2}$ (Fig. S4 and Scheme S1, ESI†).[9,15c] The TCF acceptors were condensed with the bisaldehydes to afford the π-conjugated TCF hemicyanine precursors in good yields. We found that the change of donor and acceptor structures has great influence on the reactivity and selectivity of reactions. For **JD0**, only **TE-I-9** as a type-I product was obtained in a good yield of 54% (entry 8, Table 2), indicating relatively high π-nucleophilicity of **JD0** at the unhindered C-9 position. **JD1** with the *n*-butoxy substituent at the C-8 position is a commonly used strong electron donor for push–pull polyene chromophores.[16–18] Different from typical synthetic protocols to functionalize the julolidine moiety with an aldehyde group for condensation reactions, here we identify the unique dual reactivity of **JD1** as a hydride donor for C-2 and π-nucleophile for C-9, enabling efficient condensation with TCF-based hemicyanines. For **JD3**, introducing the 8-acetoxy groups to the donor structure led to a lower yield of **TE-II-8**, suggesting reduced reactivity of **JD3** (entry 7, Table 2).

We used thin layer chromatography (TLC) to carefully monitor the reaction and optimize the yields of products from the final condensation between **JD1** and **TCF-A1-7** (Tables S2–S6, ESI†). We found that enhanced acceptor strength from **TCF1** to **TCF5** enables faster reactions, indicating higher hydrophilicity and/or electrophilicity of π-conjugated TCF hemicyanine precursors. The optimized reaction time of the final condensation was shortened to 1 h for **TCF5** as the strongest acceptor, considerably reduced from 14 h for **TCF1** as the weakest acceptor in the series. More importantly, the change of acceptor strength has substantial impact on the selectivity of reactions. As initially discovered, the **TCF1**-based reactions gave the type-II products of **TE-II-1** and **TE-II-2** as the major products in modest yields (22–27%). **TCF2** and **TCF3** are slightly stronger acceptors than **TCF1** by introducing the substituent of phenyl derivatives at the germinal position of the structures. Compared to **TCF1**-based results, **TCF2**- and **TCF3**-based reactions gave significantly higher yields (11%) of **TE-I** chromophores, while the yields of **TE-II** chromophores remained essentially identical (around 25%, entries 2 and 3 in Table 2). **TCF4** and **TCF5** are two of strongest acceptors in the series due to the introduction of fluorinated phenyl groups at the germinal position of the TCF base structure. Their reactions demonstrated a reversed selectivity relative to the results from **TCF1**-based reactants, affording **TE-I** chromophores as the major product and **TE-II** chromophores as the minor one (Entries 5 and 6, Table 2).

We did the same level of DFT calculations for **TCF5**-based reactions (Fig. 4 and Fig. S2, ESI,† in green color) and compared the results with those of **TCF1**-based reactions (Fig. 4 and Fig. S2, ESI,† in black color). Incorporating a strong acceptor of 4-fluorophenyl (**FP**) substituted **TCF5** to the system has reduced the $\Delta G^{\ddagger}_{298}$ of **FP-TS-I-B** (28.0 kcal mol^{-1}) by 1.0 kcal mol^{-1} (relative to **TS-I-B**) in the C-9 condensation (Path I). This may be due to the stabilized effect of ''additional'' halogen bonding between α hydrogens of the **JD1′** and the fluorine atom on **TCF-A6** (Fig. 4, 3D structure).

On the other hand, the **TCF5**-based pathway has a higher $\Delta G^{\ddagger}_{298}$ in the initial HT step, 27.0 kcal mol^{-1} for **TS-II-A** *vs.* 30.3 kcal mol^{-1} for **FP-TS-II-A** (Fig. 4). In the **FP-TS-II-A**, although a halogen bonding effect also exists between two reactants, the steric hindrance, which forces **JD1′** to do a

rotation displacement, may play an important role and results in a higher $\Delta G^{\ddagger}_{298}$ value (Fig. 4, 3D structure).

Further examination on the atomic charge of **TCF-A2** (Fig. S1, ESI†) indicates that the carbon (0.036) on the central ethylene bears a similar positive charge to the carbon (0.053) next to the ethoxy terminal. It appears that the conjugation length to the TCF correlates with a smaller $\Delta G^{\ddagger}_{298}$ of the **TS-II-A(c)**, 25.5 kcal mol^{-1} *vs.* 27.0 kcal mol^{-1} of the **TS-II-A**. The **TCF5**-based **TCF-A6** is expected to display a higher electrophilicity and lower $\Delta G^{\ddagger}_{298}$'s in the initial HT step, especially at the much more positively charged carbon (0.397) of the central ethylene. The DFT results show that the condensation reaction following the HT-PT process occurs at the central ethylene of **TCF-A2** and **TCF-A6** (Fig. S3, ESI†) and is rate-determining due to a higher PES.

Since a change of 1.4 kcal mol^{-1} in standard Gibbs free energy of formation (ΔG^{0}_{298}) changes the equilibrium constant by approximately a factor of 10, the DFT analysis can well explain the essential features of experimental results, such as reversed selectivity and reactivity change with the change of acceptor strength. The TH reactivity of two C=C double bonds of TCF-based hemicyanines and relatively high barriers for a few key steps may explain the limited yields of products. Overall, the remarkable correlation shown between experimental and computational results supports the adequacy of DFT calculations used in this work and provides key insight into the reaction mechanisms for further improvement of yields. Also, the study presents an unprecedented example of catalyst-free TH sequentially from two C(sp^3) hydrogens of a strong electron donor to the double bond of highly polarizable hemicyanines assisted by noncovalent π–π interactions, which is fundamentally different from the common catalytic or direct TH reactions *via* a six-membered cyclic transition state for HT.[1,3]

Crystal structures, solvatochromic, electrochemical, and thermal properties of chromophores

The crystal structures of **TE-II-1**, **TE-II-2**, **TE-I-6**, and **TE-II-6** were obtained using a slow evaporation method of the compound in a mixed solvent of chloroform and ethanol. This series of chromophores all crystallize in a centrosymmetric space group (Tables S7–S10 and Fig. S87–S90, ESI†). While the structures of **TE-II-1**, **TE-II-2**, and **TE-I-6** contain *s-trans* conformation of TCF acceptors, the structure of **TE-II-6** shows *s-cis* conformation of the TCF acceptor with reversed bond length alternation (BLA), which is very rare among all the reported crystal structures of TCF-based push–pull chromophores.[8–10,15] This could be contributed by the unique ring-locked structure of the isojuloline donor and conformation of acceptor moiety, both in *s-cis* conformation, inducing highly efficient intramolecular charge transfer (ICT) of **TE-II-6** to form a polar (zwitterionic) ground state in the crystal structure.

The solvatochromic and electrochemical properties of these chromophores were measured to understand the ICT of new push–pull structures (Fig. 5 and Fig. S85, ESI†). We select the compounds with reasonable solubility in the measurements. These chromophores, both type-I and type-II, feature a near-Gaussian-like broad absorption band and positive solvatochromism in nonpolar solvents such as toluene and trichloroethylene,

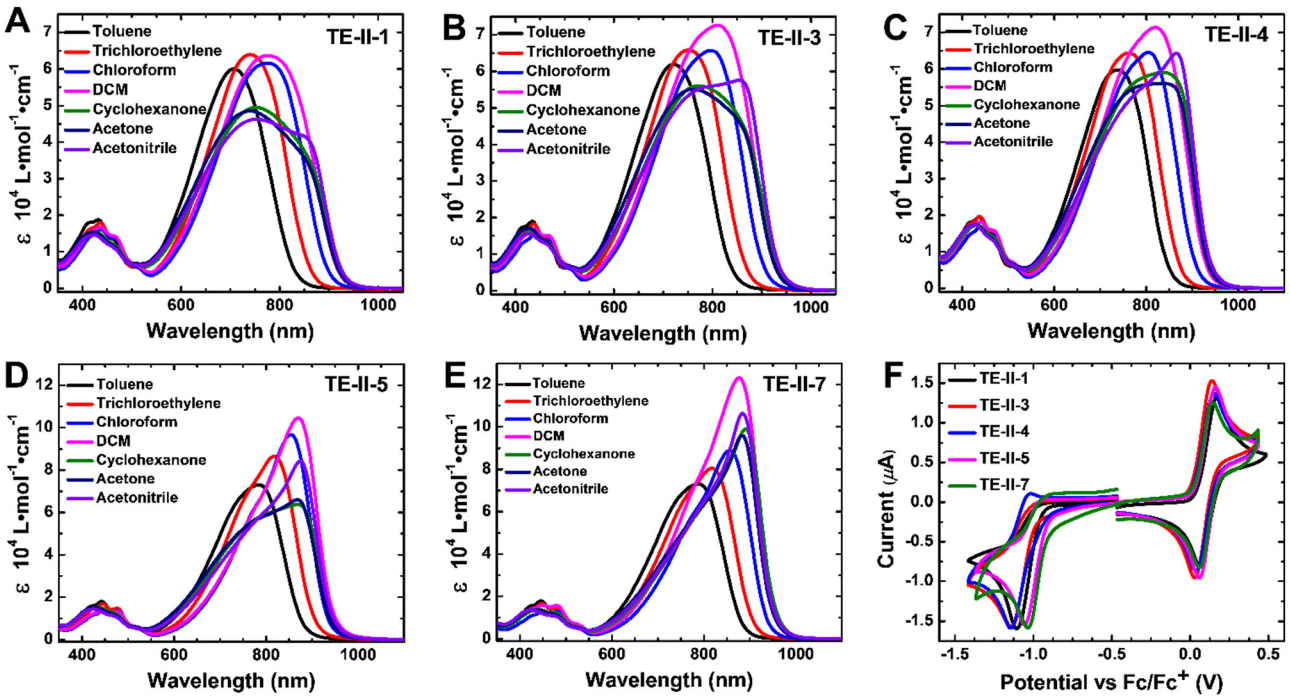

Fig. 5 (A)–(E) UV-vis-NIR spectra of type-II chromophores recorded in solvents of different polarities. (F) Cyclic voltammograms of type-II chromophores in degassed anhydrous DCM solutions containing 0.1 M tetra-butylammonium hexafluorophosphate (TBAPF) as the supporting electrolyte.

suggesting the neutral ground state (NGS) of chromophores. In polar solvents from DCM to acetonitrile, type-I chromophores showed the same broad absorption bands and inverted solvatochromism for the polar (zwitterionic) ground state (ZGS) of chromophores, while the type-II chromophores displayed a substantial change in absorption band shape with the appearance of long-wavelength shoulders or main peaks at 850–900 nm. For **TE-II-5** and **TE-II-7** with strong TCF acceptors, larger extinction coefficients of relatively sharp peaks may point to an increased contribution from a cyanine-like resonance structure or ideal polymethine state (IPS) to the electronic structures of chromophores.[28] Herein the IPS can also be treated as arising from equal contributions of NGS and ZGS resonance structures.[10] The solvatochromism data of this study show that the electronic structures of new push–pull chromophores could be primarily governed by two resonance structures of NGS ↔ ZGS for type-I products, and by three resonance structures of NGS ↔ IPS ↔ ZGS for type-II products, respectively.[15–17]

Cyclic voltammetry (CV) measurements were conducted in dichloromethane solutions to determine the electrochemical properties of chromophores (Fig. 5F and Fig. S85F, ESI†). From the relative oxidation and reduction potentials of chromophores, the HOMO levels of type-I chromophores were about −4.94 eV, slightly deeper than the −4.90 eV of type-II chromophores, both different from the typical value of −4.85 eV for TCF-based push–pull heptamethines containing **F1**, **F2**, and **M1** donors.[15] The LUMO levels of these chromophores varied from −3.73 eV for the **TCF1** acceptor to −3.83 eV for the **TCF5** acceptor. The analysis shows that new chromophores from this modular one-pot synthetic method adds a unique feature of fine-tuned energy levels to the molecular systems of push–pull phenyltrienes and heptamethines.

The thermal stability of chromophores was evaluated by TGA and the results are shown in Fig. S86 (ESI†). Except for **TE-II-5**, these chromophores show a high decomposition temperature (T_d), with the onset T_d greater than 200 °C, promising for potential photonic applications in phototheranostics and optoelectronics.

EO property study of chromophores in poled polymers

An immediate outcome of synthetic chemistry from this study is to evaluate the nonlinear optical (NLO) properties of new chromophores in solid state. Therefore, optical quality thin films of guest–host polymers were prepared with a loading density (N) of chromophores at 1.30×10^{20} cm^{-3}. Poly(styrene-*co*-methyl methacrylate) (P(S-*co*-MMA)) was used as the host polymer for its excellent optical and dielectric properties, and good compatibility with TCF-based dipolar chromophores. The films were poled under the electric field of 100 V μm^{-1}. A prism-coupler system Metricon 2010/M was used to measure the field-induced optical birefringence and calculate the r_{13} and r_{33} values of poled films in slab waveguide geometry.[15,29] Table 3 summarized the experimental results of poled polymers, including the maximum absorption wavelength (λ_{max}), r_{33} values at 1.3 μm, refractive indices of the transverse electric (TE) and transverse magnetic (TM) modes, and order parameters. It should be noted that the electric field of TM modes has two components that are in the plane of and perpendicular to the film surface for correct r_{33} calculation.[29b] The $\beta_\mu(-\omega;\omega,0)$ values of chromophores at 1304 nm were calculated by following the convention of the rigid oriented gas model (ROGM).[30,31] Two previously reported push–pull heptamethines with comparable optical bandgap, **F1** and **F2**, were included for comparison.

We found that type-I and type-II chromophores exhibited comparable NLO properties in poled polymers. The obtained r_{33} values of poled guest–host polymers at 1304 nm were relatively large while maintaining rather blue-shifted absorption bands of chromophores. The NLO activities of two types of chromophores differed considerably with the change of acceptor strength. For type-I series, optimal r_{33} values around 67 pm V^{-1}, corresponding to the largest β_μ values from this study, were demonstrated for **TE-I-5** and **TE-I-7** containing stronger **TCF4** and **TCF5** acceptors, respectively. For type-II series, however, the best r_{33} value and corresponding β_μ value were achieved for **TE-II-1** containing a simple **TCF1** acceptor and the values gradually dropped for **TE-II-3**, **TE-II-4**, and **TE-II-5**,

Table 3 NLO properties of chromophores in poled guest–host films[a]

Chromophore	λ_{max} in nm	n_{TE}/n_{TM} at 1304 nm	n_{TE}/n_{TM} at 1541 nm	r_{33}, pm V^{-1} at 1304 nm	Φ^b	β_μ, 1.3[c] μm (10^{-30} esu)
TE-I-1	678	1.5592/1.5733	1.5534/1.5581	29.1	0.08	2103
TE-II-1	754	1.5680/1.5853	1.5609/1.5787	46.3	0.10	2931
TE-I-3	698	1.5643/1.5797	1.5585/1.5757	43.7	0.09	2838
TE-II-3	767	1.5730/1.5954	1.5652/1.5840	47.6	0.14	2799
TE-I-4	712	1.5681/1.5853	1.5613/1.5758	37.9	0.10	2673
TE-II-4	804	1.5759/1.5958	1.5670/1.5878	37.1	0.11	2330
TE-I-5	740	1.5681/1.5904	1.5601/1.5784	67.1	0.11	4106
TE-II-5	854	1.5832/1.6093	1.5726/1.5953	29.9	0.13	1718
TE-I-7	752	1.5742/1.5989	1.5661/1.5832	65.1	0.11	4106
F1[d]	835	1.5840/1.6233	1.5702/1.6022	23.1	0.155	1273
F2[d]	863	1.5748/1.6184	1.5645/1.5905	27.4	0.19	1332

[a] A loading density of chromophores at 1.30×10^{20} cm^{-3} and the host polymer poly(styrene-*co*-methyl methacrylate) were used to formulate the guest–host systems. [b] The order parameters of poled films were calculated from the poling-induced optical birefringence of n_{TE} and n_{TM} with a Sellmeier fit of refractive indices. [c] The β_μ is the vector part of β tensors along the dipole moment direction of chromophores and was calculated using the rigid oriented gas model (ROGM). [d] Data of two previously reported heptamethine chromophores, **F1** and **F2**, were included for comparison.[15a] See Fig. 2 for detailed structures, where X = Cl, R = *tert*-butyl, and $\mathbf{R^1}$, $\mathbf{R^2}$ = methyl.

despite their red-shifted absorption bands and large order parameters with stronger acceptors. The results corroborate the electronic structures of these chromophores that are governed by the relative contribution of difference resonance forms, as revealed by the solvatochromism study.

At the wavelength of 1.3 μm, the NLO activities of new type-I and type-II chromophores are much higher than those from known push–pull heptamethines with similar optical bandgaps, improving the β_μ values by 165% for **TE-I-1** *vs.* **F1** and 308% for **TE-I-7** *vs.* **F2**.[15a] Interestingly, the order parameters of these new chromophores were lower than those of **F1** and **F2**, suggesting room for further improvement of the material's performance. On the other hand, the resulting reduced optical birefringence for the poled films would be beneficiary to the polarization-independent operation of poled polymers in optical waveguides.[32]

Conclusions

In summary, we have discovered that strong electron donor 8-alkoxyjulolidines exhibit unique dual reactivity of a hydride donor at the C-2 position and π-nucleophile at the C-9 position in the synthesis of push–pull chromophores, enabling exceptional reactivity and selectivity with TCF-based hemicyanines. Beside the normal condensation at C-9, DFT calculations and experimental data support the intermolecular α-HT from one C(sp^3)–H bond at C-2 of julolidine derivatives to the acceptor moiety as the key initial step, followed by β-deprotonation to generate a nucleophilic enamine of isojuloline that condenses *in situ* with a second equivalent of π-conjugated TCF hemicyanine electrophiles. The simple condition of the reaction cascade represents an unprecedented example of TH from the α- and β-C(sp^3) hydrogens of 8-alkoxyjulolidine donor to TCF-based hemicyanines, notably under simple reaction conditions without using potent catalysts of metal complexes or Lewis acids. Furthermore, DFT calculations have provided critical insight into the reaction pathways and transition states and the results are remarkably consistent with the experimental results in how the changes of donor and acceptor structures can influence the reactivity and selectivity of reactions. The products of both julolidine- and isojuloline-based push–pull chromophores exhibit strong near-infrared (NIR) absorption, good stability and large first hyperpolarizabilities. The study suggests that TH reactions between strong electron donors to highly polarizable π-acceptors can be exploited to construct new NIR merocyanines by following rational, regioselective condensation pathways for photonic applications.

Conflicts of interest

There are no conflicts to declare.

Acknowledgements

This work was supported by the National Natural Science Foundation of China (U20A20165), the Guangdong-Hong Kong-Macao research team projects of Guangdong Basic and Applied Basic Research Foundation (2020B1515130006), the Research Grants Council (RGC) of Hong Kong (RGC ref no. 11306320, 11307020, 11303721, and 11317922), the Fundamental Research Project funding from Shenzhen Science & Technology Innovation Committee (JCYJ20180507181718203), and internal research supports or initiatives from City University of Hong Kong (9610454 and 9678261). The computational studies were carried out using the computational facilities at Burgundy at City University of Hong Kong. The authors thank Dr Ken S. M. Yiu and Dr Man-Kit Tse, both at the Department of Chemistry of City University of Hong Kong, for single-crystal crystallography and 2D NMR analysis, respectively.

Notes and references

1 (*a*) D. Wang and D. Astruc, The golden age of transfer hydrogenation, *Chem. Rev.*, 2015, **115**, 6621–6686; (*b*) W. Fang and A. Riisager, Recent advances in heterogeneous catalytic transfer hydrogenation/hydrogenolysis for valorization of biomass-derived furanic compounds, *Green Chem.*, 2021, **23**, 670–688.

2 (*a*) W. Zuo, A. J. Lough, Y. F. Li and R. H. Morris, Amine(imine)diphosphine iron catalysts for asymmetric transfer hydrogenation of ketones and imines, *Science*, 2013, **342**, 1080–1083; (*b*) P. O. Lagaditis, P. E. Sues, J. F. Sonnenberg, K. Y. Wan, A. J. Lough and R. H. Morris, Iron(II) complexes containing unsymmetrical P–N–P′ pincer ligands for the catalytic asymmetric hydrogenation of ketones and imines, *J. Am. Chem. Soc.*, 2014, **136**, 1367–1380; (*c*) R. Bigler, R. Huber and A. Mezzetti, Highly enantioselective transfer hydrogenation of ketones with chiral $(NH)_2P_2$ macrocyclic iron(II) complexes, *Angew. Chem., Int. Ed.*, 2015, **127**, 5260–5263; (*d*) N. Ishida, Y. Kamae, K. Ishizu, Y. Kamino, H. Naruse and M. Murakami, Sustainable system for hydrogenation exploiting energy derived from solar light, *J. Am. Chem. Soc.*, 2021, **143**, 2217–2220; (*e*) I. Chatterjee and M. Oestreich, Brønsted acid-catalyzed transfer hydrogenation of imines and alkenes using cyclohexa-1,4-dienes as dihydrogen surrogates, *Org. Lett.*, 2016, **18**, 2463–2466.

3 T. K. Das, A. M. R. Treviño, S. Pandiri, S. Irvankoski, J. H. Siitonen, S. M. Rodriguez, M. Yousufuddin and L. Kürti, Catalyst-free transfer hydrogenation of activated alkenes exploiting isopropanol as the sole and traceless reductant, *Green Chem.*, 2023, **25**, 746–754.

4 X. Xu, X. Li, L. Ma, N. Ye and B. Weng, An unexpected diethyl azodicarboxylate-promoted dehydrogenation of tertiaryamine and tandem reaction with sulfonyl azide, *J. Am. Chem. Soc.*, 2008, **130**, 14048–14049.

5 A. Labed, F. Jiang, I. Labed, A. Lator, M. Peters, M. Achard, A. Kabouche, Z. Kabouche, G. V. M. Sharma and C. Bruneau, Iridium-catalyzed sustainable access to functionalized julolidines through hydrogen autotransfer, *ChemCatChem*, 2015, **7**, 1090–1096.

6 (*a*) X.-D. An and J. Xiao, Recent advances in hydride transfer-involved C(sp^3)-H activation reactions, *Org. Chem. Front.*, 2021, **8**, 1364–1383; (*b*) L. Wang and J. Xiao, Hydrogen-atom transfer reactions, *Top. Curr. Chem.*, 2016, **374**, 17.

7 (*a*) F. Jiang, M. Achard and C. Bruneau, Vicinal α,β-functionalizations of amines: cyclization versus dehydrogenative hydrolysis, *Chem. – Eur. J.*, 2015, **21**, 14319–14323; (*b*) B. Xiong, Y. Li, W. Lv, Z. Tan, H. Jiang and M. Zhang, Ruthenium-catalyzed straightforward synthesis of 1,2,3,4-tetrahydronaphthyridines via selective transfer hydrogenation of pyridyl ring with alcohols, *Org. Lett.*, 2015, **17**, 4054–4057; (*c*) R. Li, Y. Chen, K. Jiang, F. Wang, C. Lu, J. Nie, Z. Chen, G. Yang, Y.-C. Chen, Y. Zhao and C. Ma, $B(C_6F_5)_3$-catalyzed redox-neutral β-alkylation of tertiary amines using p-quinone methides via borrowing hydrogen, *Chem. Commun.*, 2019, **55**, 1217–1220; (*d*) L. Zhou, Y.-B. Shen, X.-D. An, X.-J. Li, S.-S. Li, Q. Liu and J. Xiao, Redox-neutral β-C(sp^3)-H functionalization of cyclic amines via intermolecular hydride transfer, *Org. Lett.*, 2019, **21**, 8543–8547.

8 W. Bentoumi, J.-C. Mulatier, P.-A. Bouit, O. Maury, A. Barsella, J.-P. Vola, E. Chastaing, L. Divay, F. Soyer, P. L. Barny, Y. Bretonnière and C. Andraud, Concise multigram-scale synthesis of push-pull tricyanofuran-based hemicyanines with giant second-order nonlinearity: an alternative for electro-optic materials, *Chem. – Eur. J.*, 2014, **20**, 8909–8913.

9 J. Luo, F. Lin, Z.-A. Li, M. Li, T.-D. Kim, S.-H. Jang and A. K.-Y. Jen, New push-pull polyene chromophores containing a michler's base donor and a tricyanofuran acceptor: multicomponent condensation, allopolar isomerism and large optical nonlinearity, *J. Mater. Chem. C*, 2017, **5**, 2230–2234.

10 S. Pascal, Y. A. Getmanenko, Y. Zhang, I. Davydenko, M. H. Ngo, G. Pilet, S. Redon, Y. Bretonnière, O. Maury, I. Ledoux-Rak, S. Barlow, S. R. Marder and C. Andraud, Design of near-infrared-absorbing unsymmetrical polymethine dyes with large quadratic hyperpolarizabilities, *Chem. Mater.*, 2018, **30**, 3410–3418.

11 J. Chan, S. C. Dodani and C. J. Chang, Reaction-based small-molecule fluorescent probes for chemoselective bioimaging, *Nat. Chem.*, 2012, **4**, 973–984.

12 H. Li, D. Kim, Q. Yao, H. Ge, J. Chung, J. Fan, J. Wang, X. Peng and J. Yoon, Activity-based NIR enzyme fluorescent probes for the diagnosis of tumors and image-guided surgery, *Angew. Chem., Int. Ed.*, 2021, **60**, 17268–17289.

13 C. Xu and K. Pu, Second near-infrared photothermal materials for combinational nanotheranostics, *Chem. Soc. Rev.*, 2021, **50**, 1111–1137.

14 (*a*) X. Li, D. Zhang, G. Lu, T. He, Y. Wan, M. K. Tse, C. Ren, P. Wang, S. Li, J. Luo and C. S. Lee, Photochemical synthesis of nonplanar small molecules with ultrafast nonradiative decay for highly efficient phototheranostics, *Adv. Mater.*, 2021, **33**, 2102799; (*b*) G. Deng, H. Chen, J. Wang, K. Chen, L. Li, S. Zhang, K. Sun, Z. Li and J. Liu, Molecular engineering of organic small-molecule photothermal agents by changing the donor group for photothermal therapy and photoacoustic imaging of tumors, *Mater. Chem. Front.*, 2022, **6**, 1180–1187.

15 (*a*) D. Zhang, J. Zou, W. Wang, Q. Yu, G. Deng, J. Wu, Z.-A. Li and J. Luo, Systematic study of the structure-property relationship of a series of near-infrared absorbing push-pull heptamethine chromophores for electro-optics, *Sci. China: Chem.*, 2021, **64**, 263–273; (*b*) D. Zhang, W. Chen, J. Zou and J. Luo, Critical role of non-classical intermolecular hydrogen bonding in affecting the π–π stacking and nonlinear optical properties of tricyanofuran-based push-pull heptamethines, *Chem. Mater.*, 2021, **33**, 3702–3711; (*c*) D. Zhang, J. Zou, W. Chen, S.-M. Yiu, M.-K. Tse, J. Luo and A. K.-Y. Jen, Efficient, stable, and scalable push-pull heptamethines for electro-optics, *Chem. Mater.*, 2022, **34**, 3683–3693; (*d*) W. Chen, T. Liu, J. Zou, D. Zhang, M. K. Tse, S. W. Tsang, J. Luo and A. K.-Y. Jen, Push-pull heptamethines near the cyanine limit exhibiting large quadratic electro-optic effect, *Adv. Mater.*, DOI: **10.1002/adma.202306089**; (*e*) X.-H. Zhou, J. Luo, J. A. Davies, S. Huang and A. K.-Y. Jen, Push-pull tetraene chromophores derived from dialkylaminophenyl, tetrahydroquinolinyl and julolidinyl moieties: optimization of second-order optical nonlinearity by fine-tuning the strength of electron-donating groups, *J. Mater. Chem.*, 2012, **22**, 16390–16398.

16 J. Wu, W. Wang, N. Wang, J. He, G. Deng, Z. Li, X. Zhang, H. Xiao and K. Chen, Structure-property analysis of julolidine-based nonlinear optical chromophores for the optimization of microscopic and macroscopic nonlinearity, *Phys. Chem. Chem. Phys.*, 2018, **20**, 23606–23615.

17 (*a*) Y. He, L. Chen, H. Zhang, Z. Chen, F. Huo, B. Li, Z. Zhen, X. Liu and S. Bo, A novel bichromophore based on julolidine chromophores with enhanced transferring efficiency from hyperpolarizability β to electro-optic activity, *J. Mater. Chem. C*, 2018, **6**, 1031–1037; (*b*) H. Zhang, H. Xiao, F. Liu, F. Huo, Y. He, Z. Chen, X. Liu, S. Bo, L. Qiu and Z. Zhen, Synthesis of novel nonlinear optical chromophores: achieving enhanced electro-optic activity and thermal stability by introducing rigid steric hindrance groups into the julolidine donor, *J. Mater. Chem. C*, 2017, **5**, 1675–1684; (*c*) Z. Zeng, J. Liu, T. Luo, Z. Li, J. Liao, W. Zhang, L. Zhang and F. Liu, Electro-optic crosslinkable chromophores with ultrahigh electro-optic coefficients and long-term stability, *Chem. Sci.*, 2022, **13**, 13393–13402.

18 J. O. S. Varejão, E. V. V. Varejão and S. A. Fernandes, Synthesis and derivatization of julolidine: a powerful heterocyclic structure, *Eur. J. Org. Chem.*, 2019, 4273–4310.

19 C. Lee, W. Yang and R. G. Parr, Development of the Colle-Salvetti correlation-energy formula into a functional of the electron density, *Phys. Rev. B: Condens. Matter Mater. Phys.*, 1988, **37**, 785–789.

20 A. D. Becke, Density-functional thermochemistry. I. The effect of the exchange-only gradient correction, *J. Chem. Phys.*, 1992, **96**, 2155–2160.

21 S. Grimme, S. Ehrlich and L. Goerigk, Effect of the damping function in dispersion corrected density functional theory, *J. Comput. Chem.*, 2011, **32**, 1456–1465.

22 F. Weigend and R. Ahlrichs, Balanced basis sets of split valence, triple zeta valence and quadruple zata valence

quality for H to Rn: design and assessment of accuracy, *Phys. Chem. Chem. Phys.*, 2005, **7**, 3297–3305.

23 (*a*) X. Xu and X. Li, Copper/diethyl azodicarboxylate mediated regioselective alkynylation of unactivated aliphatic tertiary methylamine with terminal alkyne, *Org. Lett.*, 2009, **11**, 1027–1029; (*b*) X. Xu, Z. Ge, D. Cheng, L. Ma, C. Lu, Q. Zhang, N. Yao and X. Li, CuCl/CCl4-promoted convenient synthesis of sulfonyl amidines from tertiary amines and sulfonyl azides, *Org. Lett.*, 2010, **12**, 897–899; (*c*) S. B. Bang and J. Kim, Efficient dehydrogenation of 1,2,3,4-tetrahydroquinolines mediated by dialkyl azodicarboxylates, *Synth. Commun.*, 2018, **48**, 1291–1298.

24 S. Miertuš and J. Tomasi, Approximate evalutions of the electrostatic free energy and internal energy changes in solution processes, *Chem. Phys.*, 1982, **65**, 239–245.

25 S. Miertuš, E. Scrocco and J. Tomasi, Electrostatic interaction of a solute with a continuum. A direct utilization of AB initio molecular potentials for the prevision of solvent effects, *Chem. Phys.*, 1981, **55**, 117–129.

26 J. Zheng, X. Xu and D. G. Truhlar, Minimally augmented Karlsruhe basis sets, *Theor. Chem. Acc.*, 2011, **128**, 295–305.

27 (*a*) C. C. Barker and G. Hallas, Steric effects in di- and triarylmethanes. Part IX. Electronic absorption spectra of julolidine(2,3,6,7-tetrahydro-1H,5H-benzo[ij]quinolizine) and kairoline (1-methyl-1,2,3,4-tetrahydroquinoline) analogues of Michler's hydrol blue, malachite green, crystal violet, and Michler's ketone, *J. Chem. Soc. B: Phys. Org.*, 1969, 1068–1071; (*b*) G. Hallas, N. Saadatjou, J. D. Hepworth, D. A. Ibbitson, A. M. Jones, T. P. Keane and A. R. Turton, Dipole moments of derivatives of 4-phenylazo-NN-diethylaniline and of 9-phenylazojulolidine (9-phenylazo-2,3,6,7-tetrahydro-1H,5H-benzo[ij]quinolizine), *J. Chem. Soc., Perkin Trans.*, 1981, **2**, 1292–1294.

28 (*a*) F. Meyers, S. R. Marder, B. M. Pierce and J. L. Brédas, Electric field modulated nonlinear optical properties of donor-acceptor polyenes: sum-over-states investigation of the relationship between molecular polarizabilities (α, β, and γ) and bond length alternation, *J. Am. Chem. Soc.*, 1994, **116**, 10703–10714; (*b*) P.-A. Bouit, C. Aronica, L. Toupet, B. Le Guennic, C. Andraud and O. Maury, Continuous symmetry breaking induced by ion pairing effect in heptamethine cyanine dyes: beyond the cyanine limit, *J. Am. Chem. Soc.*, 2010, **132**, 4328–4335; (*c*) A. A. Ishchenko, A. V. Kulinich, S. L. Bondarev and V. N. Knyukshto, Photodynamics of polyene-polymethine transformations and spectral fluorescent properties of merocyanine dyes, *J. Phys. Chem. A*, 2007, **111**, 13629–13637.

29 (*a*) W. Wang, J. Wu, K. Chen, Q. Huang, J. Luo and K. S. Chiang, Graphene electrodes for electric poling of electro-optic polymer films, *Opt. Lett.*, 2020, **45**, 2383–2386; (*b*) M. Dumont, Y. Levy and D. Morichere, Electrooptic organic waveguides: optical characterization, in *Organic Molecules for Nonlinear Optics and Photonics*, Dordrecht: Springer, Netherlands, 1991; 461–480.

30 M. G. Kuzyk, in *Characterization Techniques and Tabulations for Organic Nonlinear Optical Materials*, ed. M. G. Kuzyk and C. W. Dirk, Marcel Dekker, Inc., 1998, ch. 3, pp. 111–220.

31 (*a*) K. D. Singer, M. G. Kuzyk and J. E. Sohn, Second-order nonlinear-optical processes in orientationally ordered materials: relationship between molecular and macroscopic properties, *J. Opt. Soc. Am. B*, 1987, **4**, 968–976; (*b*) D. M. Burland, R. D. Miller and C. A. Walsh, Second-order nonlinearity in poled-polymer systems, *Chem. Rev.*, 1994, **94**, 31–75; (*c*) M. Stähelin, B. Zysset, M. Ahlheim, S. R. Marder, P. V. Bedworth, C. Runser, M. Barzoukas and A. Fort, Nonlinear optical properties of push-pull polyenes for electro-optics, *J. Opt. Soc. Am. B*, 1996, **13**, 2401–2407.

32 (*a*) M.-C. Oh, W. Y. Hwang and K. Kim, Transverse-electric/transverse-magnetic polarization converter using twisted optic-axis waveguides in poled polymers, *Appl. Phys. Lett.*, 1997, **70**, 2227–2229; (*b*) Y. Enami, M. Kawazu, A. K.-Y. Jen, G. Meredith and N. Peyghambarian, Polarization-insensitive transition between sol-gel waveguide and electrooptic polymer and intensity modulation for all-optical networks, *J. Light Technol.*, 2003, **21**, 2053–2060; (*c*) X. Sun and F. Qiu, Polarization independent high-speed spatial modulators based on an electro-optic polymer and silicon hybrid metasurface, *Photonics Res.*, 2022, **10**, 2893–2900; (*d*) T. Lian, K. Yang, S. Sun, M. Zhu, J. Yue, B. Lin, X. Sun, X. Wang and D. Zhang, Polarization-independent electro-absorption optical modulator based on trapezoid polymer-graphene waveguide, *Opt. Laser Technol.*, 2022, **149**, 107815.

